Two Phase Brushless D.C. Motor For Artificial Heart Applications

ABDEL-KARIM DAUD

Electrical and Computer Engineering Department
Palestine Polytechnic University (PPU)
P.O. Box 198 Hebron, Tel:+972-2-2228912, Fax:+972-2-2217248
PALESTINE
Email: daud@ppu.edu

Abstract:- The paper presents a performance analysis of brushless d.c. motor (BLDCM) with two air gap windings for a left ventricular heart assist system. The medical system consists of a bloodpump, a centrifugal pump, a brushless d.c. motor, a solenoid, power supply and controls. The brushless d.c. motor operates sensorless and is developed with respect to the special requirements of an implantable heart assist device. Here should be investigated the effect of rotor magnet design on artificial heart driving motor performance, in which rotors with different magnet lengths or thicknesses, as well as different peripheral angles, were designed and simulated in the same motor stator with different rotating speeds. This simulation is based on the calculation of the air-gap flux density of the motor, which is obtained by using three dimensional analytical field method. Then the motor efficiency was computed. MATLAB was used to implement the procedures to calculate the required parameters. The results demonstrated that the reduction of rotor magnet size and the enlargement of the air gap between the rotor magnets and the stator coil core have no significant effect on motor efficiency, but will reduce the torque value on which the motor achieves the highest efficiency; it could be remedied however by increasing the rotating speed, because the torque at the high efficiency point will increase along with the rotating speed. These results may provide a basis for developing small rotor magnets, large air gap and high efficiency motors for driving an artificial heart pump.

Key-Words:- Heart Assist System, BLDCM, Permanent Magnets, Sensorless Control, MATLAB

1 Introduction

The artificial heart (or heart assist system) finds more and more applications and has been the subject of much research in recent years. Usually, it is a type of centrifugal blood pump driven by a motor. There are left ventricular and right ventricular heart assist systems available. A left ventricular assist device pumps the blood from the left apex into the aorta and could be helpful in 80% of cases, where heart transplantation is necessary. Because of risk of infection a heart assist device have to be totaling implantable. Therefore a highly durable and reliable system with smallest possible volume and weight is required. The left ventricular heart assist system is made up of a blood pump, a centrifugal pump, a brushless d.c. motor, a solenoid, power supply and controls as shown in Fig.1 [1, 2,3]. The highly efficient brushless d.c. motor drives the centrifugal pump.

In order to reduce the size and weight of the pump, improvement of the motor design was of greatest importance. The simplest way of minimizing the motor is to reduce the magnet size of the rotor and to investigate its effect on the torque and the efficiency of the motor. The results are applied successfully in designing a new mini motor for an artificial heart pump device.
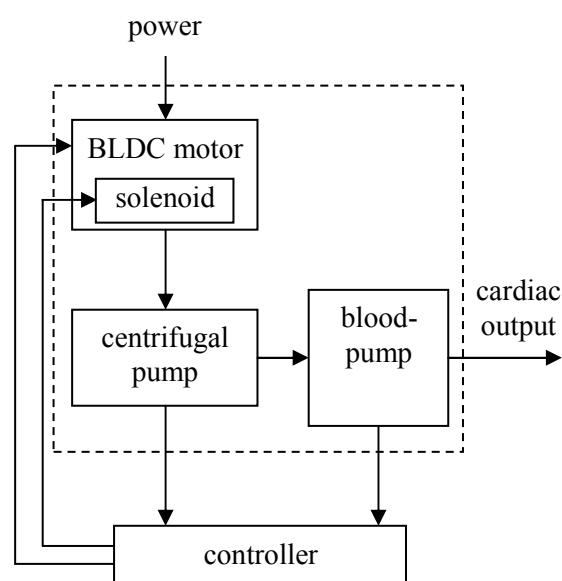
Fig.1: Block diagram of drive system

Permanent-magnet excited brushless dc motors (BLDCM) are becoming increasingly attractive in many applications due to their performance advantages such as reduced size and weight, high efficiency, low noise and maintenance, improved reliability and very good control characteristics in a wide speed range [12,14,17,18].

The most popular brushless DC motors have three-phase windings [8, 9] or four-phase windings [11], which are controlled and driven by full bridge transistor circuit [13]. From these classical types of brushless dc motor with three or four windings, it became clear that the electronic circuit is still expensive so that this type of motor could not be used in consumer applications.

In this paper, a brushless DC motor with two air gap windings and PM-rotor in different arrangement is investigated [5]. Therefore, the cost of the electronic circuit is reduced.

There are also other types of brushless dc motor with one phase [6, 7]. They have a complex construction with high ripple and reluctance torque; therefore such motors are not suitable for this application.

Elimination of position and velocity transducers in dc drives is desirable for a number of reasons. The shaft transducers themselves and perhaps even more the associated wiring, are a significant source of failure and cost. However, for a good performance of the PM dc motor, the rotor position has to be known with high accuracy. Much effort, reflected in the numerous papers dealing with this issue, has been made in research to avoid use of a position sensor in dc drives [10, 15, 16]. In this paper, the detection of back-emf technique is used.

The air gap flux density is obtained by using a three dimensional analytical method [4]. By using MATLAB, the different motor parameters and characteristics are determined.

2 Motor Design and its Drive Circuit

A total implantable system requires a drive with small volume and weight. The specific parameters are: 824 *kW/m3* and 5896 *Nm/m3*. The bloodpump operates at high speeds (5000 ... 7000 *rpm)* combined with high torque (15 ... 20 *mNm)* [1]. The developed motor with a very small mass of magnets and its air-gap windings operates in the required high speed- and torque-range. For an optimal design of the motor an analytical method has been developed. The aim is to find out the best design parameters for the optimal use of the available volume and to reach the highest efficiency at the systolic operating point (6000 rpm, 15 mNm).

The block diagram of a two-pole, two-phase brushless dc motor drive is shown in Fig.3, while the basic construction of this motor is shown in Fig.2.
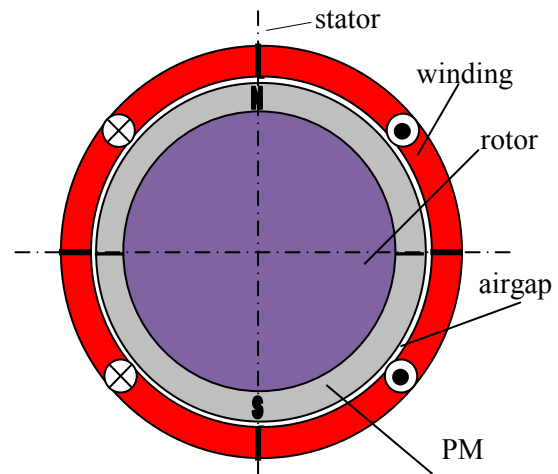
Fig. 2: Construction of BDCM
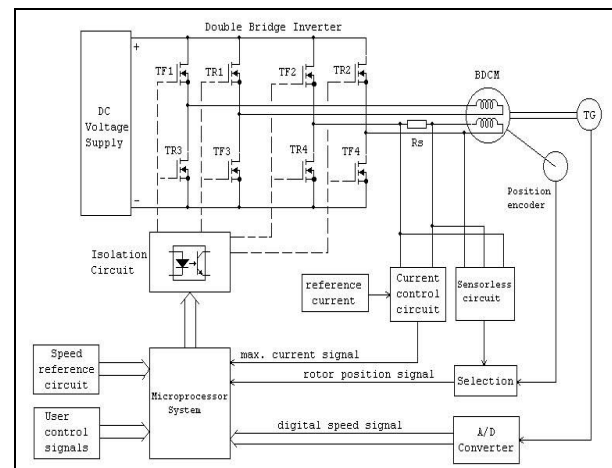
Fig.3: Drive circuit of two phase brushless DC motor

The electromagnetic structure of the drive system, as shown in Fig.2, is formed of an internal rotor ring formed permanent magnet arrangement, and a slotless stator assembly that consists of a lamination stack with air gap windings. The construction and distribution of stator windings are shown in Figs.4 and 5. The motor has two phases. Each phase consists of four coils. These coils combine two parallel groups. Each group consists of two series coils at the same radius as shown in Fig.4.

Therefore, the first phase has the two parallel groups: (A0.0, B0.0) and (A1.0, B1.0), while the remaining coils (A0.5, B0.5) and (A1.5, B1.5) combine the second one.
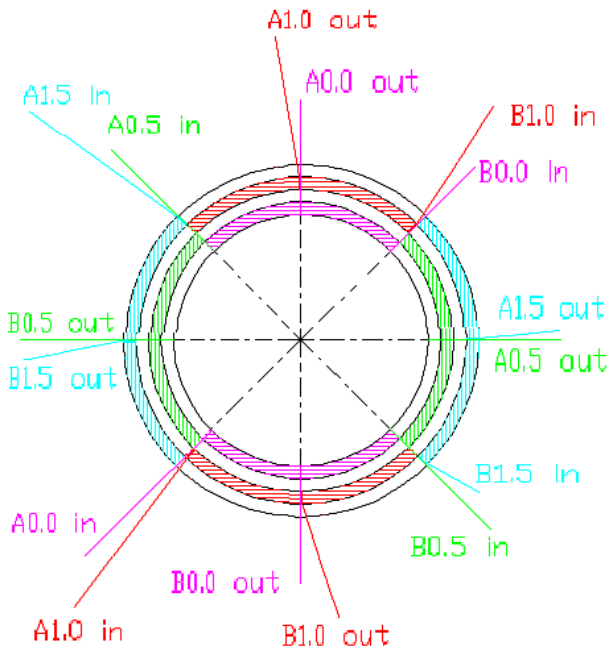
Fig. 4: Construction of stator windings
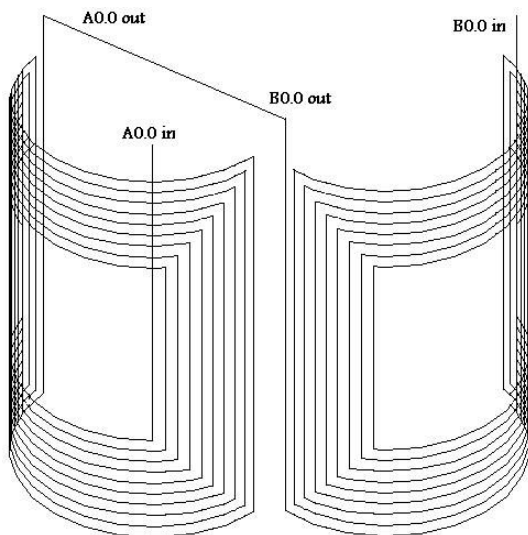
Fig. 5: One group-phase connection

In this case, the current will flow in each phase for a period of about (180°) for every rotor revolution. An increase in the number of phases will only provide a slight increase in the average torque, but it requires more power switches for the electronic commutation circuit. The power converter, as shown in Fig. 3, is a double bridge circuit (inverter) that provides the required sequence of the phase voltages in both directions [9]. The powers MOSFETs receive their gate signals from the microprocessor through the 8155 PID interface circuit. Detection of the rotor position can be achieved through photocell or sensorless control circuit.
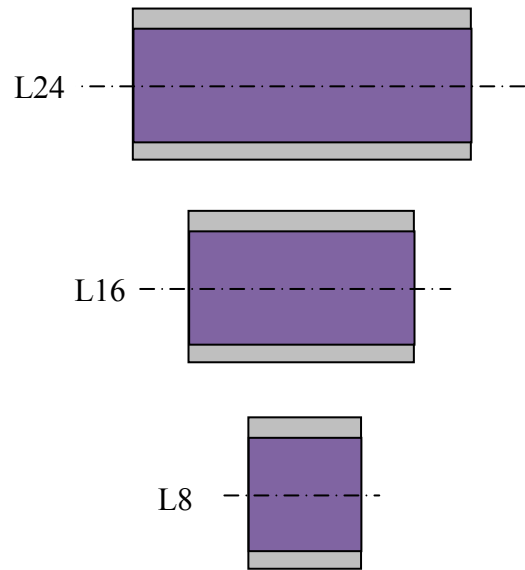
Fig.6: Rotor magnets with different axial length
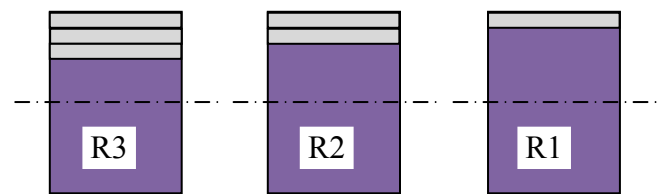
Fig. 7: Rotor magnets with radial thickness
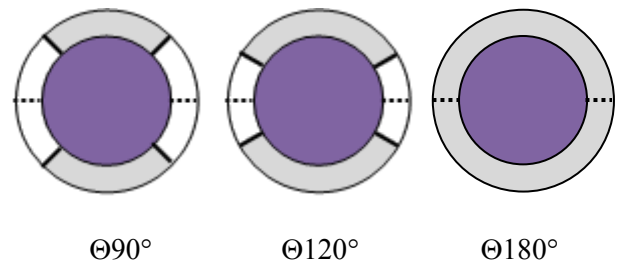
Fig.8: Rotor magnets with different peripheral angles
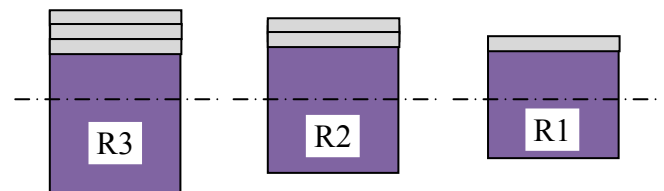
Fig. 9: Rotor magnets with radial thickness with different air gaps

Several rotor arrangements were considered. They have different axial lengths of 24 mm (L24), 16 mm (L16) and 8 mm (L8) respectively (Fig. 6), or

different radial thickness of 3 mm (R3), 2 mm (R2) and 1 mm (R1) separately (Fig. 7), as well as different peripheral angels of 180° (Θ180),120° (Θ120) and 90° (Θ90) (Fig.8). Therefore, a rotor described as L24R3Θ180 means that this rotor magnet has 24 mm axial length, 3 mm radial thickness and 180° peripheral angles. Many rotor magnets were used in the simulation; they are L24R3Θ180, L24R3Θ120, L24R3Θ90, L16R3Θ180, L16R3Θ120, L16R3Θ90, L24R2Θ180, L24R1Θ180 and L8R3Θ180.

For the previous rotor arrangements (Fig. 7), the air gap between the rotor magnets and the stator coil core is considered to be constant.

According to Fig. 9, the air gap between the rotor magnets and the stator coil core can be enlarged 1mm radially by use of R2 (δ1) and 2 mm by use of R1 (δ2) and reducing the rotor radius, as compared with R3. δ1 means that, the air gap is enlarged 1mm radial. That is to say, it is necessary to consider the effect of both the rotor magnet size and the air gap on motor performance during changes of the rotor magnet thickness. Therefore, additional rotor magnets were used in the simulation: L24R2Θ180δ1 and L24R1Θ180δ2.

These rotors were simulated in the same motor stator coil.

3 Air Gap Flux Density

The air-gap flux density B_δ is obtained from a three dimensional analytical method in the author' field calculation, which is based on Bio-Savarat-law by using mirror laws under the influence of the iron yoke [4].

4 System Model

Fig. 10 shows the equivalent circuit for one phase. The angle α in Fig.10 will give the actual position of the rotor. During $\alpha_1 \le \alpha \le \alpha_2$ the winding is energized from the dc source with the voltage V, in which the induced voltage is positive as shown in Fig.11.

Therefore, the transistor switches on this period, which is called a current flow angle δo and given by

$$\delta o = \alpha_2 - \alpha_1 \qquad (1)$$

where α_1 and α_2 are switch-on and -off angles respectively. For the electronic switch a voltage

drop of V_T is assumed. The curve of transistor voltage V_T is represented in Fig.12.

By inspection of Fig.8:

$$V = e + R\,i + L\frac{di}{dt} + V_T \;\; \text{for } \alpha_1 \le \alpha \le \alpha_2 \qquad (2)$$

With

$$\alpha = \omega t \quad \text{and} \quad \frac{d}{dt} = \omega\frac{d}{d\alpha} \;, \qquad (3)$$

the governing equation can be arranged into the following form:

$$Ri(\alpha)+\omega L\frac{di}{d\alpha}=V-e(\alpha)-V_T(\alpha) \quad \text{for } \alpha_1 \le \alpha \le \alpha_2 (4)$$
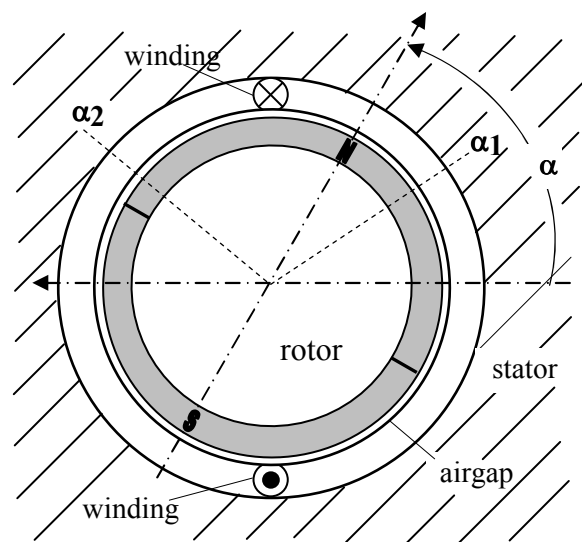
(a)
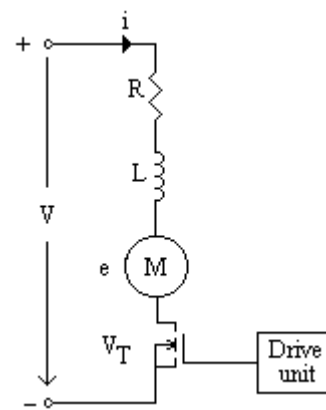
(b)

Fig.10: Drive circuit configuration of the motor
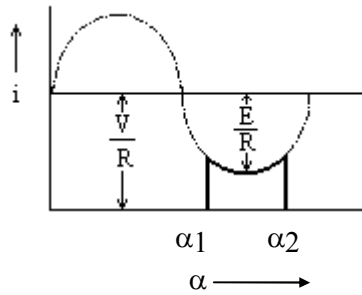
Fig.11: Phase current as function of rotor position for L $\longrightarrow$ 0
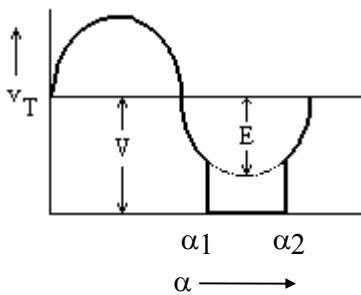
Fig.12: Transistor voltage as function of rotor position for L $\longrightarrow$ 0

5 Voltages and Currents

The magnetic flux density is obtained by applying the three dimensional field methods. Each winding is characterized by number of windings, average diameter of winding, active length and winding parameter.

Therefore the induced voltages can be written as

$$e(\alpha) = C_m \, \omega \, B_\delta(\alpha) \qquad (5)$$

where C_m is the motor constant.

Taking into account eqs. (4) and (5) and for steady state conditions, the instantaneous current can be obtained. Then the average value of the armature current can be calculated over the period $(0, 2\pi)$ and is given by:

$$I_{ave} = \frac{1}{2\pi} \int_o^{2\pi} \sum_{j=1}^{N} i_j(\alpha) d\alpha \qquad (6)$$

where N is the number of armature phases.

6 Torque

The gross electromagnetic torque is given by [10]:

$$T = C_m \, B_\delta(\alpha) \, i(\alpha) \qquad (7)$$

In order to produce a continuous torque, two or more phases have to be energized in sequence. Therefore, the average torque T_{ave} can be calculated over the period $(0, 2\pi)$ during the current flow angle δo.

The efficiency of the drive system is

$$\eta = \frac{T_{ave} \, \omega}{V \, I_{ave}} \qquad (8)$$

7 Simulation and Results

The previous described method has been applied to a two pole, two phase brushless DC motor with air gap windings and different PM-rotor arrangements. The rotor consists of a high energy sintered Nd-Fe-B magnet material. The special feature of this brushless DC motor is that no rotor position sensors, such as Hall probes or magnetoresistive sensors, are used. For detection of rotor position the induced voltage is used in combination with an electronic circuit. A three dimensional analytical method was used for field calculations.

The simulation of the transient and steady-state characteristics of the motor was carried out using the well-known software package MATLAB. The instantaneous air-gap flux density B_δ is shown in Figs.12, 13, 14 and 15. The rotor magnet length has significance only for low values of magnet length (L=8mm) according to Fig. 12. While different magnet peripheral angles have effect on the shape and values of air-gap flux density B_δ as shown in Fig. 13. It is clear; the values of B_δ are smaller by decreasing the angle. The rotor magnet radial thickness has a great effect on the flux density distribution B_δ as shown in Fig. 14.The shape and values of B_δ are lower by decreasing magnet thickness for constant air gap length. That means, these values will be very lower by enlarging the air gap length as shown in Fig. 15.
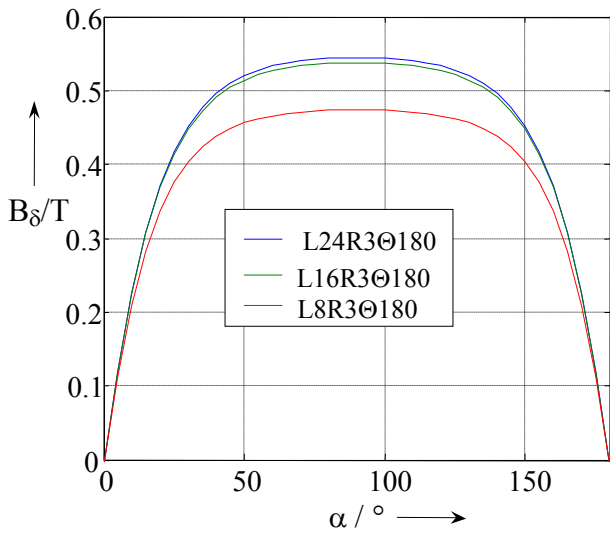
Fig. 12: B_δ distribution for different magnet length

Fig. 13: B_δ distribution for different magnet peripheral angles

Fig. 14: B_δ distribution for different magnet radial thickness
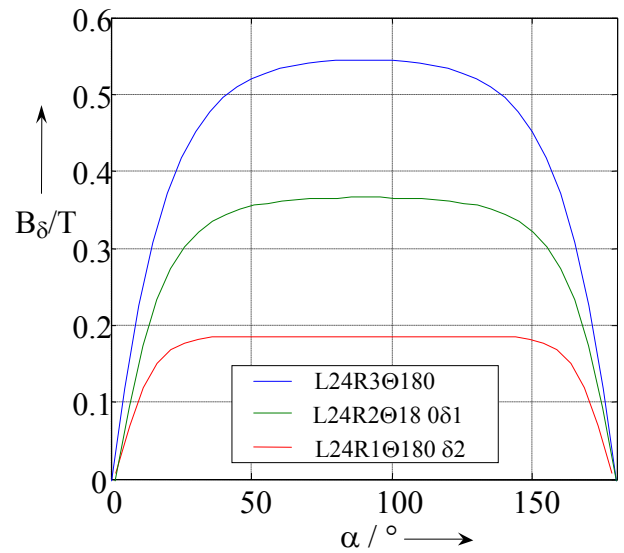
Fig. 15: B_δ distribution for different magnet radial thickness and enlarging the air gap length
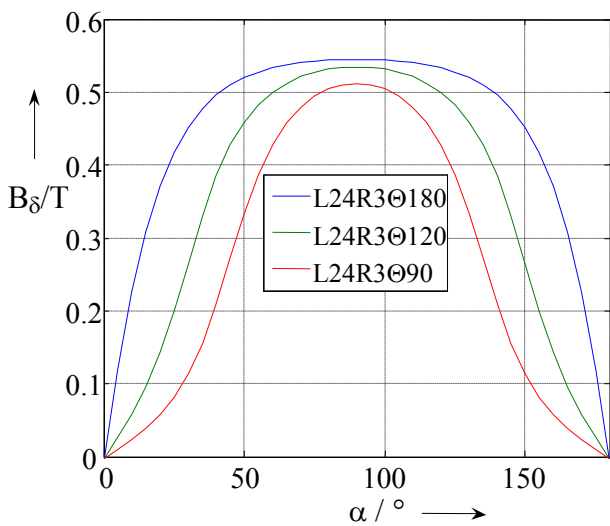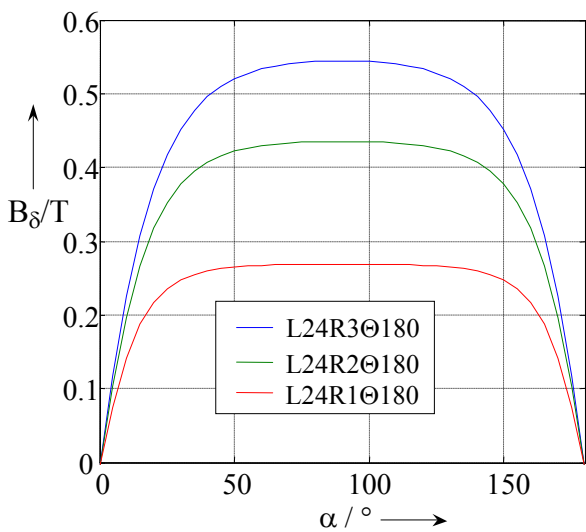
Fig. 16 demonstrates the effect of the rotor magnet axial length on the motor torque and the efficiency. The rotor magnet length has no significance on the efficiency of the motor according to Fig. 16, only the torque achieving the highest efficiency has decreased together with the rotor magnet length.

Equally, different magnet peripheral angles have also no obvious effect on motor efficiency (Fig. 17), only the torque achieving the highest efficiency has decreased together with the rotor magnet peripheral angle.
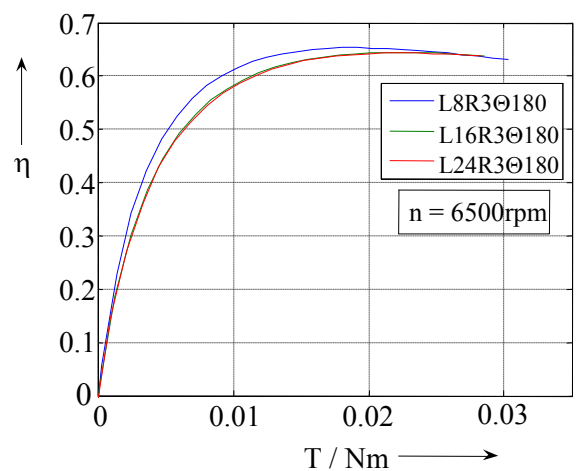
Fig. 16: Effect of rotor magnet axial length on motor torque and efficiency
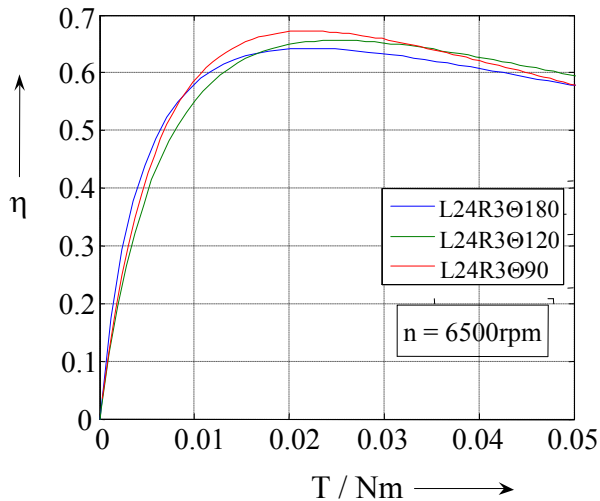
Fig. 17: Effect of rotor magnet peripheral angles on motor torque and efficiency

The rotor magnet radial thickness again has an unremarkable effect on the motor efficiency according to the curves of L24R3Θ180 and L24R2Θ180 (Fig. 18). The efficiency of the L24R1Θ180 curve has decreased, indicating that the rotor magnets could not be too thin. According to Fig. 19, the efficiencies of the L24R2Θ180δ1 and L24R1Θ180δ2 curves have more decreased, indicating that the air gap could not be too big.

It seems that the rotating speed has a very small effect on motor efficiency (Fig. 20), only the torque of the highest efficiency point increases together with the rotating speed.
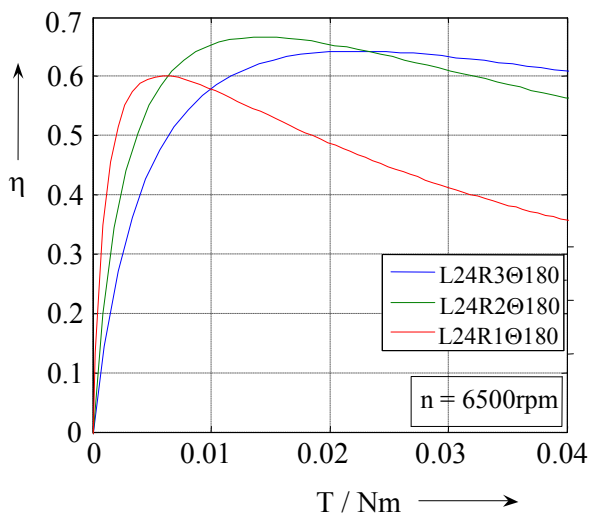
Fig. 18: Effect of rotor magnet radial thickness on motor torque and efficiency
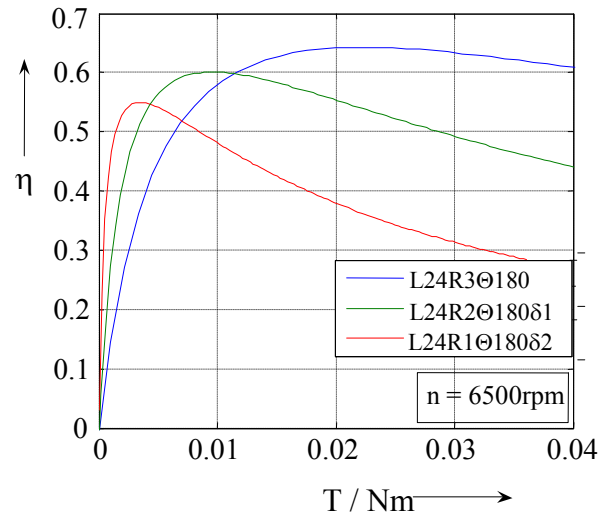
Fig. 19: Effect of rotor magnet radial thickness on motor torque and efficiency by enlarging the air gap length
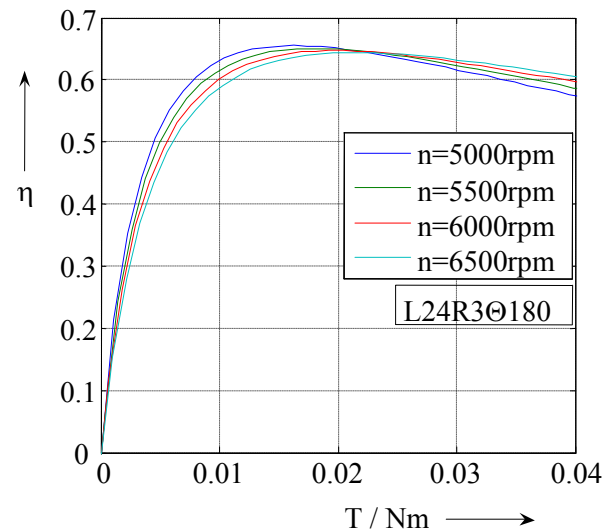
Fig. 20: Effect of rotating speed on motor torque and efficiency

8 Conclusions

This paper presented a performance analysis for a brushless DC motor with two phases for medical application. This motor type has air gap windings and different arrangements of Nd-Fe-B PM-rotor. For calculation the air-gap magnetic flux density, a three dimensional analytical method was used. With results of air gap flux density, motor

characteristics were calculated. This analytical method was used to reveal the effect of rotor magnet size (axial length, radial thickness and peripheral angle) and air gap on motor torque and efficiency. It is certified that the rotor size and air gap have no significant effect on motor efficiency, but the motor torque value at which the highest efficiency is achieved will increase along with increasing motor size and along with decreasing air gap. This means a small rotor and large air gap motor could achieve a high efficiency, but its output torque will reduce if the motor performs at its highest efficiency point or close by.

Fortunately, this shortcoming could be remedied by increasing the rotating speed of the motor, because the high efficiency point has larger output torque at higher speed than at lower speed. It is concluded that a small rotor motor with large air gap and large output torque and with high efficiency is feasible, as long as the rotating speed is high enough. The rotating speed is a very important factor for blood pump design. The motor design should therefore be performed with the pump development simultaneously.

References:

[1]   R. Hanitsch; N. Parspour, Contribution to brushless dc motor design for a heart assist device, *ICEM*, 1992, Manchester, Vol. 1 pp. 165-169.

[2]   A.C. Guyton; J. E. Hall, *Textbook of Medical Physiology*, Philadelphia, Pa, Elsevier Saunders, 2006.

[3] K. X. Qian; H. Y. Yuan; W. M. Ru; P. Zeng, Technical note: Experimental method to reveal the effect of rotor magnet size and air gap on artificial heart driving motor torque and efficiency, *Journal of Medical Engineering & Technology*, Sept./Okt. 2002, Number 5, Volume 26, pp. 199-201.

[4] A.-K. Daud, A three dimensional field analysis of permanent magnets", *The Palestinian Engineering Conference*, August 2001, Nablus, pp. 144-157.

[5] A.-K. Daud, Performance analysis of two phase brushless DC motor for sensorless operation, *WSEAS Transactions on Power Systems*, May 2006, Issue 5, Volume 1, pp. 802-809.

[6] A.-K. Daud, Analysis of sensorless controlled one phase brushless DC motor, *WSEAS Transactions on Power Systems*, March 2006, Issue 3, Volume 1, pp. 625-631.

[7] S. Khader, Single phase brushless DC motor with PWM control strategy and special form of PM motor, *Proc. of WSEAS Conference on Energy & Environmental system*, Chalkida, Greece, May 2006, pp. 218-226.

[8] A.-K. Daud; S.H. Khader, An analytical method for determination of commutation leading angle in three- phase brushless DC motor, *Proc. Of ELECTROMOTION'97*, Cluj-Napoca,   pp. 253-258.

[9] G. Baluta; N. Papachatzis, Three phase brushless DC motor: Logic sequencer and converter, *WSEAS Transactions on Systems*, September 2006, Issue 9, Volume 5, pp. 2105-2112.

[10]   H.-K. Jafari, Design and Implementation of DC motor speed controller using Fuzzy-Adaptive controller, *WSEAS Transactions on Circuits and Systems*, April 2008, Issue 4, Volume 7, pp. 203-212.

[11] R. Hanitsch, Analog computer simulation of brushless DC motors, *Proc. of ICEM*, 1984, Lausanne, pp. 189-192.

[12] J.M.D. Coey, *Rare-Earth Iron Permanent Magnets*, Oxford Science Publications, Clarendon Press Oxford, 1996.

[13]   M.H. Rashid, *Power Electronics, Circuits, Devices and Applications*, Pearson Prentice Hall, Upper Saddle River, New Jersy, 2004.

[14] H.B. Ertan; M.Y. Üctung; R. Colyer; A. Consoli, *Modern Electrical Drives*, Kluwer Academic Publishers, Netherlands, 2000.

[15] L. Harnefors; P. Taube; H.-P. Nee, An improved method for sensorless adaptive control of permanent-magnet synchronous motors, *Proc. Eur. Conf. Power Electronics*, Trondheim, Vol 4, 1997.

[16] N. Matsui, Sensorless permanent-magnet brushless DC and synchronous motor drives, *ELECROMOTION*, Vol 3, No. 4, 1996, pp. 172-180.

[17] J.D. Ede; Z.Q. Zhu; D. Howe, Design considerations for high-speed permanent magnet brushless dc motors, *Proc. International Conference on Power Electronics, Machines, and Drives, IEE,* 2004, pp. 686-690.

[18] B.-K. Lee; M. Ehsani, Advanced simulation model for brushless dc motor drives, *Electric Power Components and Systems*, September 2003, pp 841-868